TECHNICAL RESEARCH REPORT

Control of Hysteresis in Smart Actuators, Part I: Modeling, Parameter Identification, and Inverse Control

by Xiaobo Tan, John S. Baras

CDCSS TR 2002-8
(ISR TR 2002-54)

CENTER FOR DYNAMICS AND CONTROL OF SMART STRUCTURES

Control of Hysteresis in Smart Actuators, Part I:
Modeling, Parameter Identification, and Inverse Control

Xiaobo Tan[*] and John S. Baras

Institute for Systems Research and

Department of Electrical and Computer Engineering

University of Maryland, College Park, MD 20742 USA

{xbtan, baras}@isr.umd.edu

Abstract

Hysteresis in smart actuators presents a challenge in control of these actuators. A fundamental idea to cope with hysteresis is inverse compensation. In this paper we study modeling, identification and inverse control of hysteresis in smart actuators through the example of controlling a commercially available magnetostrictive actuator. The (rate-independent) Preisach operator has been used extensively to model the hysteresis in smart actuators. We present efficient inversion algorithms for the Preisach operator that are implementable in real-time. The magnetostrictive hysteresis is rate-dependent at high frequencies. For this we propose a novel dynamic hysteresis model by coupling a Preisach operator to an ordinary differential equation. This model can capture the dynamic and hysteretic behavior of the magnetostrictive actuator, and it provides insight into modeling of rate-dependent hysteresis in other smart materials. The effectiveness of the identification and inverse control schemes is demonstrated through extensive experimental results.

Keywords: Hysteresis; Smart actuators; Preisach operator; Modeling; Parameter identification; Inverse compensation

[*]Corresponding author.

1 Introduction

Smart materials, such as magnetostrictives, piezoelectrics, electroactive polymers (EAPs), shape memory alloys (SMAs), electrorheological (ER) fluids and magnetorheological (MR) fluids, all display certain coupling phenomena between applied electromagnetic/thermal fields and their mechanical/rheological properties. Actuators and sensors made of these materials can be built into structures, often called *smart structures*, with the ability to sense and respond to environmental changes to achieve desired goals. Smart materials and smart structures have been receiving tremendous interest in the past two decades, due to their broad applications in areas of aerospace, manufacturing, defense, and civil infrastructure systems, to name a few. Hysteresis widely existing in smart materials, however, makes the effective use of smart actuators and sensors quite challenging [1]. In this paper and its sister paper [2], we study modeling and control of hysteresis in smart actuators, through the example of controlling a commercially available thin magnetostrictive actuator.

Magnetostriction is the phenomenon of strong coupling between magnetic properties and mechanical properties of some ferromagnetic materials (e.g., Terfenol-D): strains are generated in response to an applied magnetic field, while conversely, mechanical stresses in the materials produce measurable changes in magnetization. This phenomenon can be used for actuation and sensing. Magnetostrictive actuators have applications to micro-positioning, robotics, ultrasonics, vibration control, etc. Figure 1 shows a sectional view of a Terfenol-D actuator manufactured by Etrema Products, Inc. By varying the current in the coil, we vary the magnetic field in the Terfenol-D rod and thus control the motion of the rod head. To give some idea about the performance of magnetostrictive actuators, we list some specifications for the AA-050H series actuators manufactured by Etrema [3]: Terfenol-D rod length 50 mm, maximum dynamic force $\pm$ 220 N, displacement range 50 μm. Figure 2 displays the hysteresis observed in the magnetostrictive actuator.

A fundamental idea in coping with hysteresis is to formulate the mathematical model of hysteresis and use inverse compensation to cancel out the hysteretic effect. This idea can be found in [5, 6, 7, 8, 9, 10]. There have been a few monographs devoted to modeling of hysteresis and study of dynamical systems with hysteresis [11, 12, 13, 14, 15].

Hysteresis models can be roughly classified into physics-based models and phenomenological models. An example of a physics-based model is the Jiles-Atherton model of ferromagnetic hysteresis [16], where hysteresis is considered to arise from pinning of domain walls on defect sites. The most popular
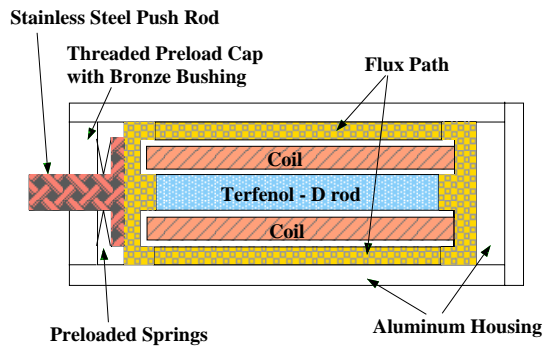
Figure 1: Sectional view of a Terfenol-D actuator [4](Original source: Etrema Products, Inc.).
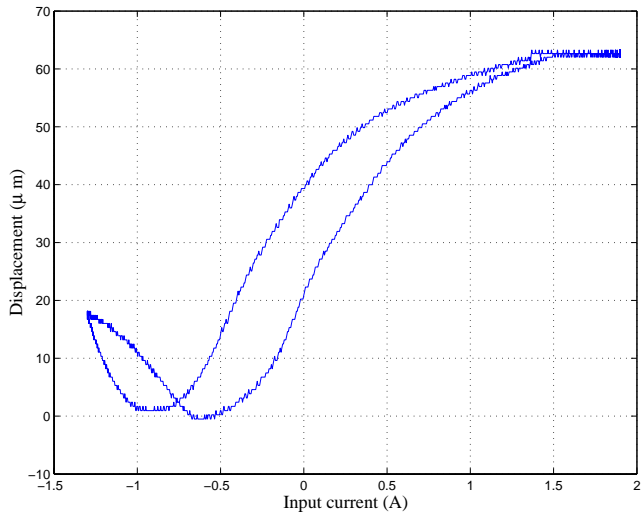

Figure 2: Hysteresis in a magnetostrictive actuator.

phenomenological hysteresis model used in control of smart actuators has been the Preisach model [17, 5, 18, 19, 20, 9, 10]. A similar type of operator, called Krasnosel'skii-Pokrovskii (KP) operator has also been used [21, 8]. Although in general the Preisach model does not provide physical insight into the problem, it provides a means of developing phenomenological models that are capable of producing behaviors similar to those of physical systems (see Mayergoyz [12] for an excellent exposition).

In this paper we study modeling, identification and inverse control methods for smart actuators. We have chosen a magnetostrictive actuator as an example for two purposes:

– The magnetostrictive hysteresis is *rate-independent* when the input frequency is low (typically below 5 Hz): roughly speaking, the shape of the hysteresis loop is independent of the rate of input variation (see Section 2 for a precise statement). The rate-independent hysteresis can be

modeled by a Preisach operator. Note that a variety of other smart actuators have been modeled by essentially a Preisach operator alone, see, e.g., [5, 20]. Therefore the identification and control methods presented here apply directly to a wide class of smart actuators.

– The magnetostrictive hysteresis is *rate-dependent* [1] when the input frequency gets high, and it can no longer be modeled by a Preisach operator alone. In this case we propose a novel dynamic hysteresis model, consisting of a Preisach operator coupled to an ordinary differential equation in an unusual way. This model captures important dynamic effects in the frequency region of practical interest. We expect our studies on rate-dependent magnetostrictive hysteresis to shed light on modeling and control of rate-dependent hysteresis in other smart materials.

The remainder of the paper is organized as follows. We provide an introduction to the Preisach operator in Section 2. Section 3 is devoted to the rate-independent case. We first discuss an identification scheme in Subsection 3.1, and then present inversion algorithms for a discretized Preisach operator and for a Preisach operator with nonsingular measure in Subsections 3.2 and 3.3, respectively. Modeling and control of rate-dependent hysteresis is addressed in Section 4. A dynamic hysteresis model is proposed in Subsection 4.1, a parameter identification method is presented in Subsection 4.2, and an inversion algorithm is given in Subsection 4.3. Finally concluding remarks are provided in Section 5.

A preliminary version of some results in this paper was presented in [22].

2 The Preisach Operator

For a pair of thresholds (β, α) with $\beta \leq \alpha$, consider a simple hysteretic element $\hat{\gamma}_{\beta,\alpha}[\cdot, \cdot]$, as illustrated in Figure 3. For $u \in C([0, T])$ and an initial configuration $\zeta \in \{-1, 1\}$, the function

$$v = \hat{\gamma}_{\beta,\alpha}[u, \zeta] : [0, T] \to \{-1, 1\}$$

is defined as follows [13]:

$$v(0) \stackrel{\triangle}{=} \begin{cases} -1 & \text{if } u(0) \leq \beta \\ \zeta & \text{if } \beta < u(0) < \alpha \\ 1 & \text{if } u(0) \geq \alpha \end{cases},$$

---

[1] In some literature, e.g., [13, 14], the word *hysteresis* is referred to rate-independent memory effects only. We use "hysteresis" in a more general sense in this paper and [2].

and for $t \in (0, T]$, setting $X_t \triangleq \{\tau \in (0, t] : u(\tau) = \beta \text{ or } \alpha\}$,

$$v(t) \triangleq \begin{cases} v(0) & \text{if } X_t = \emptyset \\ -1 & \text{if } X_t \neq \emptyset \text{ and } u(\max X_t) = \beta \\ 1 & \text{if } X_t \neq \emptyset \text{ and } u(\max X_t) = \alpha \end{cases} .$$
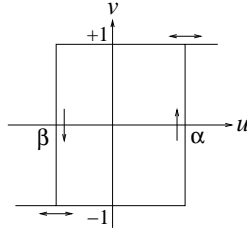

Figure 3: The elementary Preisach hysteron.

This operator is sometimes referred to as an *elementary Preisach hysteron* (we will call it a *hysteron* in this paper), since it is a building block for the Preisach operator.

The Preisach operator is a weighted superposition of all possible hysterons. Define

$$\mathcal{P}_0 \triangleq \{(\beta, \alpha) \in \mathbb{R}^2 : \beta \leq \alpha\}.$$

$\mathcal{P}_0$ is called the *Preisach plane*, and each $(\beta, \alpha) \in \mathcal{P}_0$ is identified with the hysteron $\hat{\gamma}_{\beta,\alpha}$. For $u \in C([0, T])$ and a Borel measurable initial configuration ζ_0 of all hysterons, $\zeta_0 : \mathcal{P}_0 \to \{-1, 1\}$, the output of the Preisach operator Γ is defined as [13]:

$$z(t) = \Gamma[u, \zeta_0](t) = \int_{\mathcal{P}_0} \hat{\gamma}_{\beta,\alpha}[u, \zeta_0(\beta, \alpha)](t) d\nu(\beta, \alpha), \tag{1}$$

where ν is a finite (signed) Borel measure on $\mathcal{P}_0$, called the *Preisach measure*.

In this paper we call the Preisach measure ν *nonsingular* if $|\nu|$ is absolutely continuous with respect to the two-dimensional Lebesgue measure. By the Radon-Nikodym theorem [23], if ν is nonsingular, there exists a Borel measurable function μ, such that

$$\Gamma[u, \zeta_0](t) = \int\int_{\mathcal{P}_0} \mu(\beta, \alpha) \hat{\gamma}_{\beta,\alpha}[u, \zeta_0(\beta, \alpha)](t) d\beta d\alpha. \tag{2}$$

The weighting function μ is often referred to as the *Preisach function* [12] or the *density function* [14].

To simplify the discussion, throughout the paper we assume that $\nu(E) = 0$ for any Borel measurable set

$$E \subset \{(\beta, \alpha) \in \mathcal{P}_0 | \beta < \beta_0 \text{ or } \alpha > \alpha_0\}$$

for some β_0, α_0. Then it suffices to consider a finite triangular area $\mathcal{P} \triangleq \{(\beta, \alpha) \in \mathcal{P}_0 | \beta \geq \beta_0, \alpha \leq \alpha_0\}$, as shown in Figure 4(a).

The memory effect of the Preisach operator can be captured by the *memory curves* in $\mathcal{P}$. At time t, $\mathcal{P}$ can be divided into two regions:

$$\mathcal{P}_+(t) \triangleq \{(\beta, \alpha) \in \mathcal{P} | \text{ output of } \hat{\gamma}_{\beta,\alpha} \text{ at } t \text{ is } +1\},$$
$$\mathcal{P}_-(t) \triangleq \{(\beta, \alpha) \in \mathcal{P} | \text{ output of } \hat{\gamma}_{\beta,\alpha} \text{ at } t \text{ is } -1\}.$$

Now assume that at some initial time t_0, the input $u(t_0) = u_0 < \beta_0$. Then the output of every hysteron is -1. Therefore $\mathcal{P}_-(t_0) = \mathcal{P}$, $\mathcal{P}_+(t_0) = \emptyset$ and this corresponds to the "negative saturation" (Figure 4(b)). Next we assume that the input is monotonically increased to some maximum value at t_1 with $u(t_1) = u_1$. The output of $\hat{\gamma}_{\beta,\alpha}$ is switched to $+1$ as the input $u(t)$ increases past α. Thus at time t_1, the boundary between $\mathcal{P}_-(t_1)$ and $\mathcal{P}_+(t_1)$ is the horizontal line $\alpha = u_1$ (Figure 4(c)). Next we assume that the input starts to decrease monotonically until it stops at t_2 with $u(t_2) = u_2$. It's easy to see that the output of $\hat{\gamma}_{\beta,\alpha}$ becomes -1 as $u(t)$ sweeps past β, and correspondingly, a vertical line segment $\beta = u_2$ is generated as part of the boundary (Figure 4(d)). Further input reversals generate additional horizontal or vertical boundary segments.
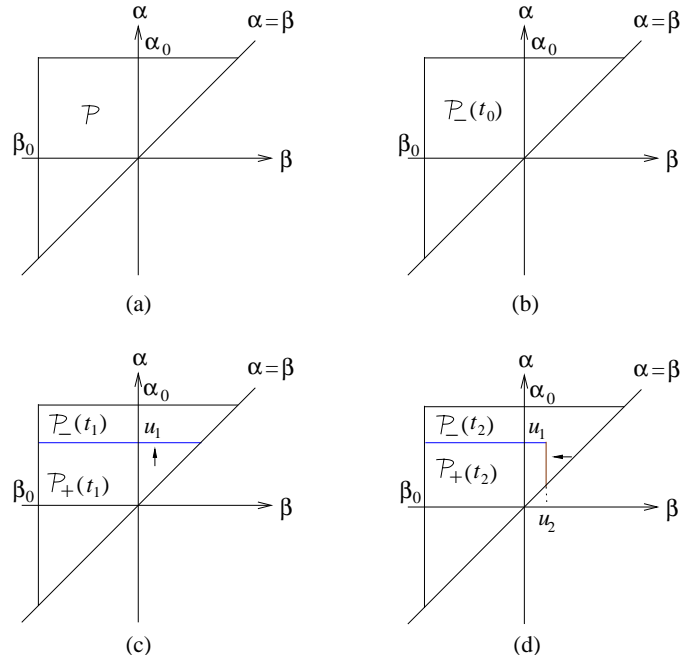

Figure 4: Memory curves in the Preisach plane.

From the above illustration, each of $\mathcal{P}_-$ and $\mathcal{P}_+$ is a connected set [12], and the output of Γ is

determined by the boundary between $\mathcal{P}_-$ and $\mathcal{P}_+$ if the Preisach measure is nonsingular. The boundary is called the memory curve. The memory curve has a staircase structure and its intersection with the line $\alpha = \beta$ gives the current input value. The memory curve ψ_0 at $t = 0$ is called the *initial memory curve* and it represents the initial condition of the Preisach operator. We denote by Ψ the *set of all memory curves*. For a precise characterization of Ψ, we refer to [24].

If the Preisach measure is nonsingular, we can identify a configuration of hysterons ζ_ψ with a memory curve ψ in the following way: $\zeta_\psi(\beta, \alpha) = 1\,(-1, \text{resp.})$ if (β, α) is below (above, resp.) the graph of ψ. Note that it does not matter whether ζ_ψ takes 1 or -1 on the graph of ψ. In the sequel we will put the initial memory curve ψ_0 as the second argument of Γ, where $\Gamma[\cdot, \psi_0] \overset{\triangle}{=} \Gamma[\cdot, \zeta_{\psi_0}]$.

Theorem 2.1 summarizes some basic properties of the Preisach operator, see, e.g., [13].

Theorem 2.1 *[13]: Let ν be a Preisach measure. Let $u, u_1, u_2 \in C([0, T])$ and $\psi_0 \in \Psi$. Then the following hold:*

1. **(Rate Independence)** *If $\phi : [0, T] \to [0, T]$ is an increasing continuous function satisfying*

$$\phi(0) = 0 \text{ and } \phi(T) = T,$$

   then $\Gamma[u \circ \phi, \psi_0](t) = \Gamma[u, \psi_0](\phi(t))$, $\forall t \in [0, T]$, where "$\circ$" denotes composition of functions.

2. **(Strong Continuity)** *If ν is nonsingular, then $\Gamma[\cdot, \psi_0] : C([0, T]) \to C([0, T])$ is strongly continuous (in the* sup *norm).*

3. **(Piecewise Monotonicity)** *Let $\nu \geq 0$. If u is either nondecreasing or noninreasing on some interval in $[0, T]$, then so is $\Gamma[u, \psi_0]$.*

4. **(Order Preservation)** *Let $\nu \geq 0$. If $u_1 \leq u_2$ on $[0, T]$, then $\Gamma[u_1, \psi_0] \leq \Gamma[u_2, \psi_0]$ on $[0, T]$.*

3 Identification and Inversion of the Preisach Operator

3.1 Identification of the Preisach operator

The only parameter of a Preisach operator is the Preisach measure. A classical method for measure identification is to use the so called *first order reversal curves* , detailed in Mayergoyz [12]. Since
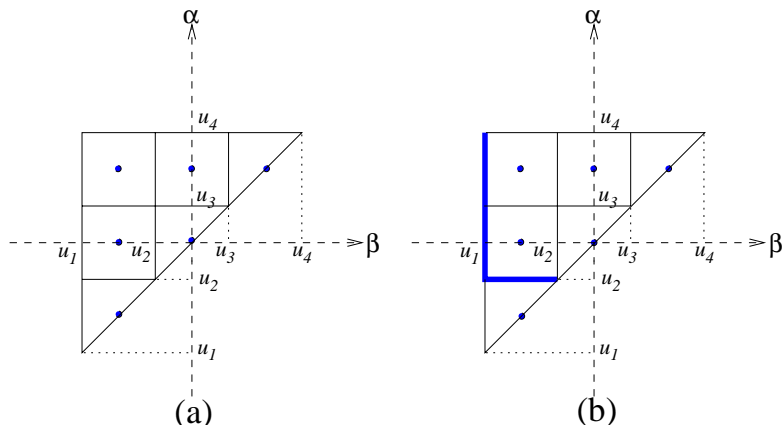
Figure 5: (a) Discretization of the (restricted) Preisach plane ($L = 3$); (b) A memory curve (represented by the bolded lines).

the method involves twice differentiation, a smooth approximating surface is fit to the data points in practice [5, 18, 20]. As pointed out in [20], deriving the density by differentiating a fitted surface is inherently imprecise, since different types of approximating functions lead to quite different density distributions. Hoffmann and his colleagues proposed a scheme to identify the Preisach measure masses for a discretized Preisach operator *directly* [25], based on which the density function is approximated in terms of a set of basis functions [26]. Another identification method is to drive the Preisach operator with a reasonably "rich" input and then determine the measure by a least squares algorithm [21, 8, 9]. Here we briefly review the identification scheme in [9].

Smart actuators, due to the capacity of the windings or other practical reasons, have to be operated with their inputs within specific ranges. As a consequence, one can only visit and identify the measure distribution in a restricted area $\mathcal{A}$ in the Preisach plane. We discretize the input range $[u_{min}, u_{max}]$ into $L + 1$ levels uniformly, and call this *discretization of level L* (see Figure 5(a) for an example of $L = 3$). The Preisach measure within each cell is assumed to concentrate as a discrete mass at the cell center (see the dark dots in Figure 5(a)). This corresponds to a discretized Preisach operator, which is weighted sum of a finite number of hysterons, as illustrated in Figure 6.

To identify the measure masses, one applies a "rich" input function $u(t)$ and measures the output trajectory $z(t)$. An input $u(t)$ is *rich* if it is able to single out the contribution of each hysteron in the discretized Preisach operator, and one candidate for such $u(t)$ is the concatenation of the first order reversal inputs. Recall that a first order reversal input is obtained by increasing the input from u_{min} to some α monotonically and then decreasing it to some β. Signals $u(t)$, $z(t)$ are sampled
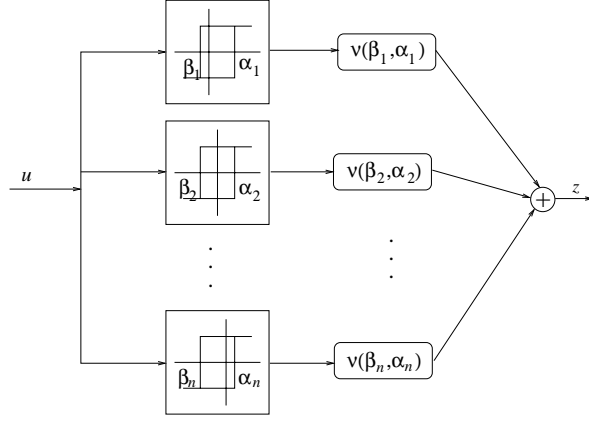
Figure 6: The discretized Preisach operator.

into sequences $\{u[n]\}_{n=1}^{N}$, $\{z[n]\}_{n=1}^{N}$. The input sequence $\{u[n]\}$ (after discretization) is fed into the discretized Preisach operator, and the state of each hysteron, $\{\hat{\gamma}_k[n]\}$, $k = 1, \cdots, K$, is then computed, where K is the number of hysterons. The output of the Preisach operator at time instant n can be expressed as:

$$\tilde{z}[n] = \Gamma[u[\cdot], \psi_0][n] = \nu_0 + \sum_{k=1}^{K} \nu_k \hat{\gamma}_k[n],\tag{3}$$

where ν_0 is the constant contribution of the Preisach measure from outside of $\mathcal{A}$, and ν_k with $k > 0$ is the measure mass corresponding to $\hat{\gamma}_k$.

Remark 3.1 *We put a sequence instead of a continuous time function as the first argument of Γ in (3). To avoid ambiguity, it is tacitly understood that the input is changed monotonically from $u[n]$ to $u[n+1]$. Throughout the paper we may use a sequence or a continuous time function as the first argument of Γ depending on the context.*

We use the least squares method to estimate the parameters, i.e., the parameters are determined in such a way that

$$\sum_{n=1}^{N} |z[n] - \tilde{z}[n]|^2\tag{4}$$

is minimized. Since we require $\nu_k \geq 0, k = 1, \cdots, K$, it is a constrained least squares problem.

Remark 3.2 *Theoretically the weighting masses can be computed directly from the first order reversal curves. This works if the signals are noise-free, which is usually not the case. Therefore we use the least squares method.*

3.1.1 Experimental results

In general the magnetostriction depends on both the mechanical pre-stress σ and the magnetic field H [17, 27]. Pre-stress is applied to the magnetostrictive actuator through preloaded springs (see Figure 1) and that improves magnetostriction. The pre-stress is not adjustable once the actuator is manufactured, and it does not change much during operation considering the magnitude of magnetostriction (less than 1500 parts per million for Terfenol-D). Therefore we assume that the magnetostriction is only dependent on the magnetic field H, which is determined by the input current I.

For the purpose of control, we define the magnetostriction λ to be

$$\lambda = \frac{\Delta l}{l_{rod}}, \tag{5}$$

where l_{rod} is the length of the magnetostrictive rod in the demagnetized state, and Δl is the change of the rod length from l_{rod}. Note that the displacement y of the actuator head is equal to Δl. The saturation magnetostriction λ_s is defined in an obvious way, which is slightly different from that in [28].

When the input frequency is low, the magnetostrictive hysteresis is rate-independent and we can relate y to the bulk magnetization M along the rod direction by a square law [4]

$$y = \frac{l_{rod}\lambda_s}{M_s^2}M^2, \tag{6}$$

and relate the input current I to the magnetic field H (assumed uniform) along the rod direction by

$$H = c_0 I + H_{bias}, \tag{7}$$

where M_s is the saturation magnetization, c_0 is the so called *coil factor*, and H_{bias} is the bias field produced by permanent magnets or a dc current. H_{bias} is necessary for generating bidirectional strains. Hence we can capture the hysteretic relationship between y and I by the ferromagnetic $M - H$ hysteresis. Venkataraman employed a low dimensional ferromagnetic hysteresis model in [4]. Here we use a Preisach operator to model $M - H$ hysteresis:

$$M = \Gamma[H, \psi_0]. \tag{8}$$

Remark 3.3 *Due to the thin rod geometry, we approximate the continuum magnetization in the magnetostrictive rod by the bulk magnetization. The square law (6) follows from the continuum theory*
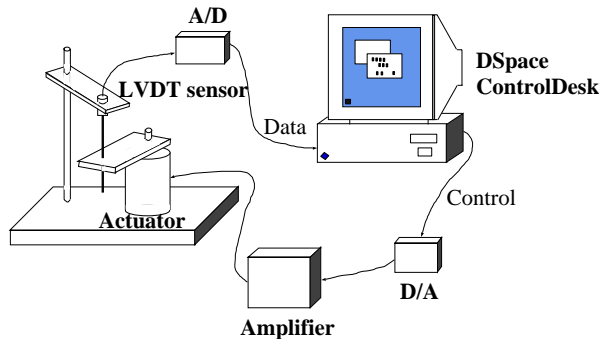
10

Figure 7: Experimental setup.

of micromagnetics, where the magnetoelastic energy is of the form linear in the strain and quadratic in the direction cosines of the magnetization vector [29].

Remark 3.4 *Mayergoyz has shown that, the necessary and sufficient conditions for a hysteretic non-linearity to be represented by a Preisach operator are the wiping-out property and the congruency property [12]. While the wiping-out property for the ferromagnetic hysteresis can be directly verified, we will indirectly verify the congruency property by a trajectory tracking experiment based on inversion of the Preisach operator.*

The following parameters are available from the manufacturer: $M_s = 7.87 \times 10^5 \text{A/m}$, $l_{rod} = 5.13 \times 10^{-2}\text{m}$, $c_0 = 1.54 \times 10^4/\text{m}$. We can easily identify $\lambda_s = 1.313 \times 10^{-3}$ by applying an input of relatively large magnitude. The bias field H_{bias} is identified to be $1.23 \times 10^4 \text{A/m}$.

Our experimental setup is as shown in Figure 7 . DSpace ControlDesk is a tool for real-time simulation and control. The displacement of the actuator is measured with a LVDT sensor, which has a precision of about 1 μm.

The magnetic field H is limited to $[1.57 \times 10^3\text{A/m}, 3.25 \times 10^4\text{A/m}]$, and we discretize the Preisach plane into 25 levels. Figure 8 shows the distribution of the identified weighting masses. The constant contribution ν_0 is estimated to be $4.99 \times 10^5\text{A/m}$.

Remark 3.5 *Due to the bias field H_{bias} and the constraint on the input current, we can not trace the major loop of the M - H hysteresis; instead we can only visit a certain region inside the major loop. As a result, the magnetostrictive hysteresis loop (the butterfly curve) is asymmetric (Figure 2).*
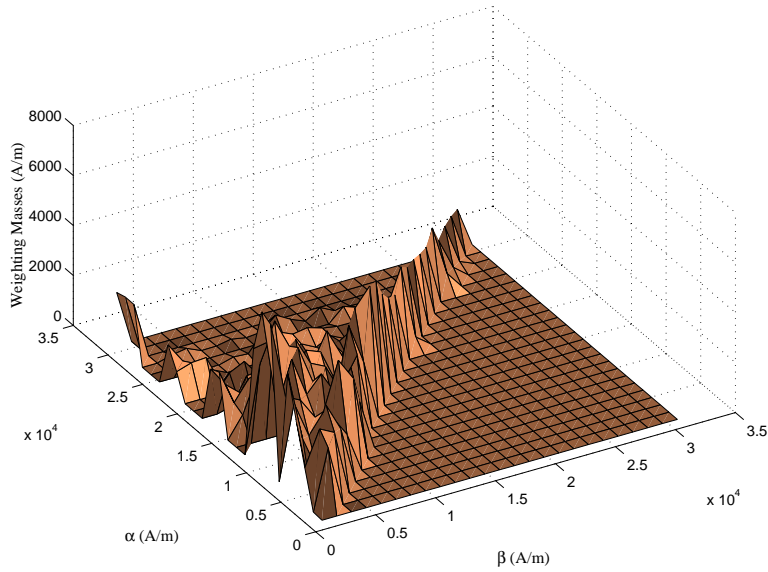
Figure 8: Distribution of the Preisach weighting masses.

3.2 Inversion of the discretized Preisach operator

General models for smart actuators that capture both hysteresis and dynamic behaviors have a cascaded structure, as shown in Figure 9. Here W is some hysteretic nonlinearity and $G(s)$ represents the transfer function of the linear part in the actuator.
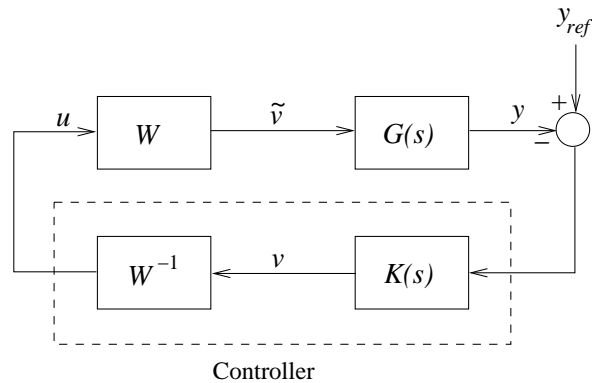

Figure 9: Controller design schematic [30].

A basic idea for controller synthesis for such systems is to construct a *right* inverse operator W^{-1} for W. Then $\tilde{v}(\cdot) = v(\cdot)$ and the controller design problem is reduced to designing a linear controller $K(s)$ for the linear system $G(s)$ (Figure 9).

The hysteretic nonlinearity W could be a rate-independent model, e.g., the Preisach operator, or

it could be a rate-dependent model, like the dynamic model to be discussed in the next section. In this subsection and the next subsection, we study inversion of the Preisach operator. Preisach operator is highly nonlinear, and in general, we can not find a closed-form formula for the inverse operator, unless the density function is of some special form, as in the work of Galinaitis and Rogers [31]. Hughes and Wen [5, 18] utilized the first order reversal curves in computing the numerical inverse of the Preisach operator. This method relies on measurement of all first order reversal curves and involves solving nonlinear equations. Natale and his colleagues proposed using another Preisach operator as a "pseudo-compensator" to approximate the inverse of a Preisach operator [10]. The compensator is "pseudo" because it is well known that in general, the inverse of a Preisach operator is not a Preisach operator. Venkataraman and Krishnaprasad proposed an inversion algorithm based on the contraction mapping principle for a Lipschitz continuous Preisach operator [30].

In this paper we exploit the piecewise monotonicity property of the Preisach operator with a nonnegative measure, and other structural properties inherited from the discretization, to develop efficient inversion algorithms which are implementable in real-time. We first study inversion of a discretized Preisach operator obtained as a result of input discretization.

Let U be the set of discrete input values, i.e., $U \triangleq \{u_l, 1 \leq l \leq L+1\}$ with

$$u_l = u_{min} + (l-1)\delta_u, \text{ where } \delta_u = \frac{u_{max} - u_{min}}{L}.$$

Let S^n be the set of input strings of length n taking values in U, i.e., if $s \in S^n$, then $s[i] \in U, 1 \leq i \leq n$. Let Ψ_d be the set of memory curves for the discretized Preisach operator. Note that any $\psi \in \Psi_d$ consists of L segments, and each segment can be either horizontal or vertical (see Figure 5(b) for an example of an element in Ψ_d with $L = 3$). Therefore, there are 2^L elements in Ψ_d.

Inversion Problem of Length N: *Let all measure masses be nonnegative. Given an initial memory curve $\psi_0 \in \Psi_d$ and a desired output sequence $\bar{z}$ of length N, find $s^* \in S^N$, such that*

$$\max_{1 \leq i \leq N} |\Gamma[s^*, \psi_0][i] - \bar{z}[i]| = \min_{s \in S^N} \max_{1 \leq i \leq N} |\Gamma[s, \psi_0][i] - \bar{z}[i]|. \tag{9}$$

Remark 3.6 *Although the Preisach measure for a discretized Preisach operator is not nonsingular, the configuration of hysterons at any time is fully captured by some memory curve in Ψ_d and we can still write $\Gamma[\cdot, \psi]$ for $\psi \in \Psi_d$.*

Remark 3.7 *A discretized Preisach operator is not "onto" since its output takes values in a finite*

set. Therefore, we do not seek an exact inverse in the problem formulation.

Before we present the solution to the problem above, we first look at the case when $N = 1$:

Inversion Problem of Length 1: *Let all measure masses be nonnegative. Given an initial memory curve $\psi_0 \in \Psi_d$ and a desired output $\bar{z}_0$, find $u^* \in U$, such that*

$$|\Gamma[u^*, \psi_0] - \bar{z}_0| = \min_{u \in U} |\Gamma[u, \psi_0] - \bar{z}_0|. \tag{10}$$

There is a simple algorithm for solving the problem of length 1, which is based on piecewise monotonicity of the Preisach operator [9]. We name it the *closest match algorithm*, because it always generates an input such that the corresponding output matches the desired output most closely among all possible inputs.

The idea of the closest match algorithm is as follows. One can obtain the initial input $u^{(0)}$ and the initial output $z^{(0)}$ from the initial memory curve ψ_0. Consider the case $z^{(0)} < \bar{z}_0$ (the case $z^{(0)} > \bar{z}_0$ is treated in exactly the same way with some obvious modification). We keep increasing the input by one level in each iteration until, say at iteration n, the input $u^{(n)}$ reaches u_{max}, or the output $z^{(n)}$ corresponding to $u^{(n)}$ exceeds $\bar{z}_0$. For the first case, the optimal input is clearly u_{max}. For the second case, two candidates for the optimal input u^* are $u^{(n-1)}$ and $u^{(n)}$, and we take u^* to be the one with smaller output error. Note that we need back up the memory curve whenever we increase the input, so that we can always retrieve the consistent memory curve with u^*.

The above algorithm yields the optimal input u^* in at most L iterations. And in each iteration, the evaluation of $z^{(n)}$ is very fast since the input has changed by one level and thus we need only update states of hysterons corresponding to that level. These factors combine to make this algorithm simple and efficient.

The trajectory inversion problem of length N is solved by combining the closest match algorithm and the dynamic programming principle.

Let $\Xi_d : \Psi_d \times U \to \Psi_d$ be the evolution map for the memory curve, i.e., if $\psi \in \Psi_d$ is the initial memory curve, then $\Xi_d(u, \psi)$ is the new memory curve when the input $u \in U$ is applied.

Given N and a desired output sequence $\bar{z}$ of length N, we define, for $1 \leq k \leq N$,

$$J_k(\psi, s) = \max_{k \leq i \leq N} |\Gamma[s, \psi][i] - \bar{z}[i]|, \ s \in S^{N-k+1}, \tag{11}$$

$$V_k(\psi) = \min_{s \in S^{N-k+1}} J_k(\psi, s), \tag{12}$$

where we call J_k the cost function and V_k the value function.

Proposition 3.1 *The value functions V_k, $1 \leq k \leq N$, can be solved successively via:*

$$V_N(\psi) = \min_{u \in U} |\Gamma[u, \psi] - \bar{z}[N]|, \tag{13}$$

$$V_k(\psi) = \min_{u \in U} \max\{|\Gamma[u, \psi] - \bar{z}[k]|, V_{k+1}(\Xi_d(u, \psi))\}. \tag{14}$$

Define maps $\pi_k^* : \Psi_d \to U$, $1 \leq k \leq N$, so that $\pi_k^*(\psi)$ is the $\arg\min$ in (13) and (14). Then for the inversion problem of length N, π_k^*, $1 \leq k \leq N$, gives the optimal control policy at time k.

Proof. Straightforward from Bellman's optimality principle [32]. $\square$

The closest match algorithm can be used in solving (13) and (14). Proposition 3.1 entails pre-computing and storage of the optimal maps, which is undesirable when N or the cardinality of Ψ_d is large. A sub-optimal approach is to decompose the inversion problem of length N into N successive inversion problems of length 1, and solve them using the closest match algorithm. Experimental results of trajectory tracking based on this approach can be found in [9].

3.3 Inversion of the Preisach operator with a nonsingular measure

We now discuss the inversion problem for a Preisach operator with a nonsingular Preisach measure. In this case, the Preisach operator can be inverted with arbitrary accuracy, and it suffices to study an inversion problem of length 1: given $\psi_0 \in \Psi$ and $\bar{M} \in [M_{min}, M_{max}]$, find $\bar{H} \in [H_{min}, H_{max}]$, such that

$$\bar{M} = \Gamma[\bar{H}, \psi_0],$$

where $[H_{min}, H_{max}]$ and $[M_{min}, M_{max}]$ are the ranges of the input and the output of the Preisach operator, respectively. The notation used in this subsection is slightly different from that in Subsection 3.2, but it will be consistent with the notation in Section 4.

Proposition 3.2 *Let the Preisach measure be nonnegative and nonsingular with a density function* μ. *Let*

$$\bar{\nu} \overset{\triangle}{=} \max\{\sup_{\alpha} \int_{\beta_0}^{\alpha} \mu(\beta, \alpha)d\beta, \ \sup_{\beta} \int_{\beta}^{\alpha_0} \mu(\beta, \alpha)d\alpha\} < \infty. \tag{15}$$

Let $\psi_0 \in \Psi$ *be the initial memory curve, and let the input and the output of the Preisach operator corresponding to* ψ_0 *be* H_0 *and* M_0, *respectively. Given* $\bar{M} \in [M_{min}, M_{max}]$, *consider the following algorithm:*

$$\begin{cases} H^{(n+1)} = H^{(n)} + \frac{\bar{M} - M^{(n)}}{\bar{\nu}} \\ M^{(n+1)} = \Gamma[H^{(n+1)}, \psi^{(n)}] \end{cases}, \tag{16}$$

where $\psi^{(0)} = \psi_0$, $H^{(0)} = H_0$, $M^{(0)} = M_0$, *and* $\psi^{(n)}$ *is the memory curve after* $\{H^{(k)}\}_{k=1}^{n}$ *is applied. Then* $M^{(n)} \to \bar{M}$ *as* $n \to \infty$.

Proof. The proposition follows directly from piecewise monotonicity and continuity of the Preisach operator. $\square$

Remark 3.8 *The algorithm (16) also appeared in [30], where approximate inversion of the Preisach operator was studied for the class of continuous, piecewise monotone functions.*

What we have identified in Subsection 3.1 is a set of Preisach weighting masses and the corresponding Preisach measure is not nonsingular. We can obtain a nonsingular Preisach measure ν_p by assuming that each identified mass is distributed uniformly over the corresponding cell in the discretization grid. Note that the diagonal cells are triangular, while other cells are square (refer to Figure 5(a)). The density function μ_p corresponding to ν_p is piecewise uniform, which enables us to solve the inversion problem exactly (in a finite number of iterations), as described next.

We consider the case $\bar{M} > M_0$ and the other case can be treated analogously. It's obvious that $\bar{H} > H_0$ and we will increase the input in every iteration. At iteration n, let $d_1^{(n)} > 0$ be such that $H^{(n)} + d_1^{(n)}$ equals the next discrete input level, and let $d_2^{(n)} > 0$ be the minimum amount such that applying $H^{(n)} + d_2^{(n)}$ will eliminate the next corner of the memory curve (see Figure 10 for illustration). Since μ_p is piecewise constant, for $d < \min\{d_1^{(n)}, d_2^{(n)}\}$, we have

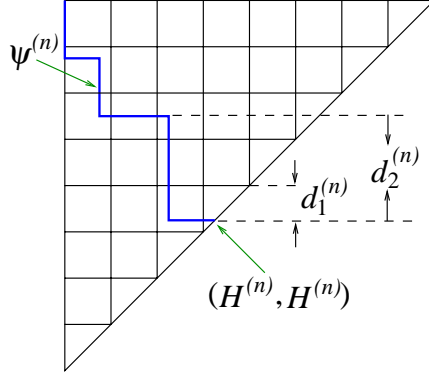$$\Gamma[H^{(n)} + d, \psi^{(n)}] - \Gamma[H^{(n)}, \psi^{(n)}] = a_2^{(n)}d^2 + a_1^{(n)}d,$$

Figure 10: Illustration of $d_1^{(n)}$ and $d_2^{(n)}$ ($L = 8$).

where $a_1^{(n)}, a_2^{(n)} \geq 0$ can be computed from μ_p, and the square term is due to the contribution from the triangular region inside the diagonal cell. Let $d_0^{(n)}$ be such that

$$\bar{M} - \Gamma[H^{(n)}, \psi^{(n)}] = a_2^{(n)}(d_0^{(n)})^2 + a_1^{(n)} d_0^{(n)}.$$

The inversion algorithm now works as follows:

$$\begin{cases} d^{(n)} = \min\{d_0^{(n)}, d_1^{(n)}, d_2^{(n)}\} \\ H^{(n+1)} = H^{(n)} + d^{(n)} \\ M^{(n+1)} = \Gamma[H^{(n+1)}, \psi^{(n)}] \end{cases} \qquad (17)$$

If at iteration n^*, $d^{(n^*)} = d_0^{(n^*)}$, then the iteration stops and $\bar{H} = H^{(n^*+1)}$. Let $n_c(\psi_0)$ be the number of corners of ψ_0, and L be the discretization level of the Preisach plane. Then it is easy to see the algorithm (17) yields the (exact) solution in no more than $\bar{n} = n_c(\psi_0) + L$ iterations.

Figure 11 shows the result of an open-loop tracking experiment using the algorithm (17). The desired trajectory was obtained from the output of a Van der Pol oscillator to make the tracking task challenging. In Figure 11, the displacement trajectories (both the desired and the measured), the tracking error, and the input current computed based on the inversion algorithm are displayed. The overall performance is satisfactory since the error magnitude is less than 3 μm most of the time with a tracking range of 60 μm. We can see that the tracking error slightly exceeds 4 μm when the desired output (and thus the input) undergoes abrupt changes, in which case the rate-independence assumption no longer holds.

The inversion problem, as discussed here and in the literature, is a *trajectory inversion* problem, since we want to find an input sequence such that the output sequence matches (most closely) the
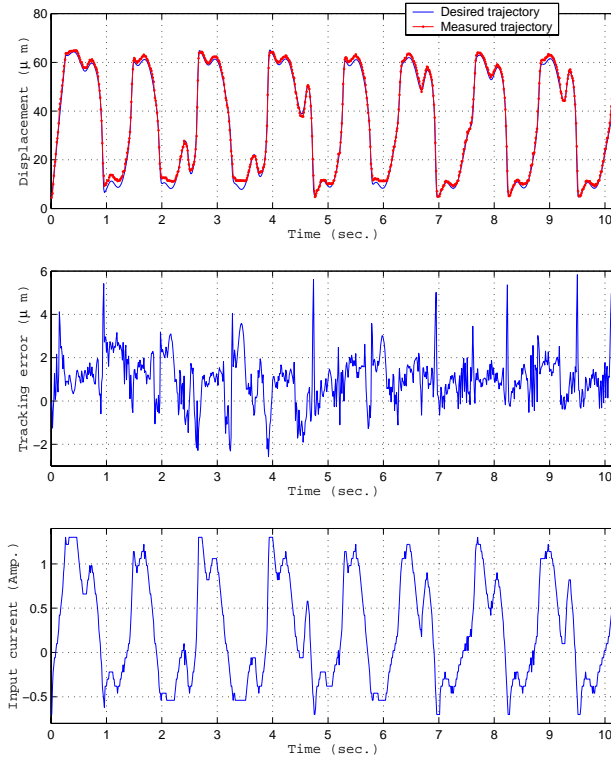
17

Figure 11: Trajectory tracking based on inversion of the Preisach operator.

desired one. In some applications, e.g., micro-positioning, one is more interested in finding an input sequence such that the *final value* of the output sequence matches (most closesly) the desired *value*. This problem, called the *value inversion* problem, was formulated and studied in [24].

4   Identification and Inversion of a Dynamic Hysteresis Model

4.1   A dynamic magnetostrictive hysteresis model

When the input frequency gets high, the magnetostrictive hysteresis is rate-dependent (Figure 12) due to the eddy current losses and the magnetoelastic dynamics of the magnetostrictive rod. Venkataraman and Krishnaprasad proposed a bulk hysteresis model for a thin magnetostrictive actuator based on energy balancing principles [33, 4]. The model has a cascaded structure as shown in Figure 13. $\bar{W}$ takes care of the M - H hysteresis and the eddy current losses, and $G(s)$ is a second order linear system modelling the magnetoelastic dynamics.
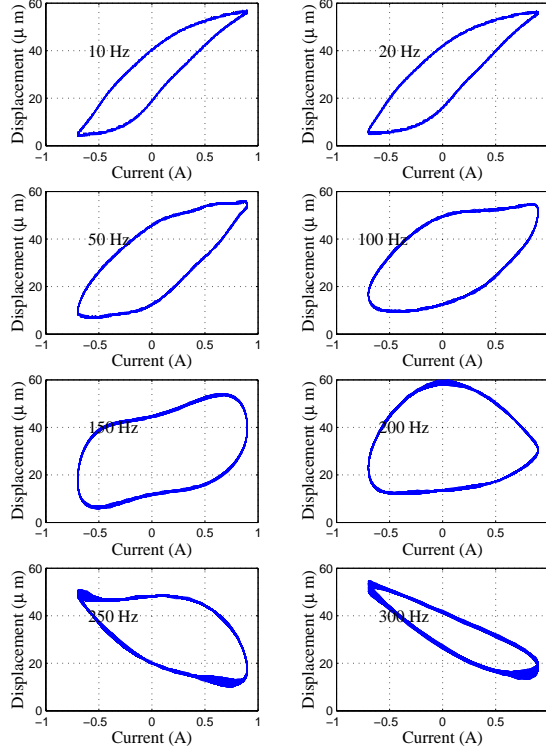
18

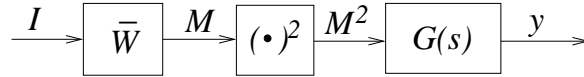Figure 12: The rate-dependent magnetostrictive hysteresis.

Figure 13: Model structure of a magnetostrictive actuator.

We now have a closer look at the block $\bar{W}$. Due to the finite resistivity of the magnetostrictive material, there are eddy currents circulating inside the rod. One way to represent the eddy current losses is to place a resistor R_{eddy} in parallel with a hysteretic inductor [28, 4], as shown in Figure 14. We note that this is a phenomenological approach and the underlying details of the eddy current dynamics are ignored here. We assume that the magnetic flux density B is uniform over the cross section of the magnetostrictive rod. Then the voltage V across the nonlinear inductor is $N_m A_m \frac{dB}{dt}$, where N_m is the number of turns of the coil, and A_m is the cross sectional area of the rod. Let I be the input current applied to the actuator, and I_1 be the current flowing in the inductor branch. Since $V = (I - I_1)R_{eddy}$, we have

$$\frac{dB}{dt} = \frac{R_{eddy}}{N_m A_m}(I - I_1). \tag{18}$$

In SI units, $B = \mu_0(H + M)$, where $\mu_0 = 4\pi \times 10^{-7}$Henry/m is the permeability of vacuum. H is related to I_1 via $H = c_0 I_1 + H_{bias}$.
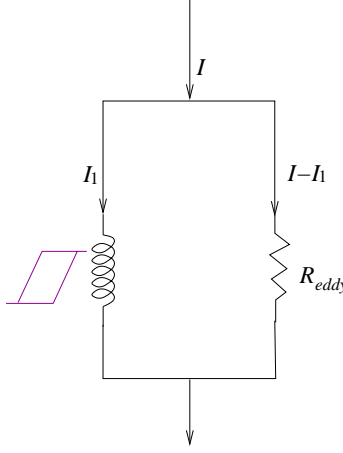
19

Figure 14: Representation of eddy current losses in a magnetostrictive actuator [4].

Remark 4.1 *Again, considering the thin rod geometry of the actuator, the continuum magnetization and the magnetic flux density are approximated by their bulk values along the rod direction, and the magnetoelastic dynamics is lumped into a second order linear system $G(s)$. Since the goal is to develop a phenomenological model suitable for real-time control applications, the approximation is necessary.*

The constitutive relationship between M and H was modeled by a low dimensional bulk ferromagnetic hysteresis model in [4] and that led to an overall model described by switching ordinary differential equations. We use a Preisach operator Γ with a nonnegative Preisach measure to model $M - H$ hysteresis and obtain the following new dynamic model for the block $\bar{W}$:

$$
\begin{cases}
\dot{H}(t) + \dot{M}(t) = c_1\left(I(t) - \frac{H(t) - H_{bias}}{c_0}\right) \\
M(t) = \Gamma[H(\cdot), \psi_0](t)
\end{cases}
,
\tag{19}
$$

where ψ_0 represents the initial memory curve and

$$
c_1 \triangleq \frac{R_{eddy}}{\mu_0 N_m A_m}.
$$

$G(s)$ has a state space representation [33, 4] (after some manipulations):

$$
\ddot{y}(t) + 2\xi\omega_0\dot{y}(t) + \omega_0^2 y(t) = \frac{\omega_0^2 l_{rod}\lambda_s}{M_s^2}M^2(t),
\tag{20}
$$

where y is the displacement, $\omega_0 = 2\pi f_0$, f_0 is the first resonant frequency of the actuator, ξ is the damping coefficient, l_{rod} is the length of the rod, λ_s is the saturation magnetostriction and M_s is the saturation magnetization.
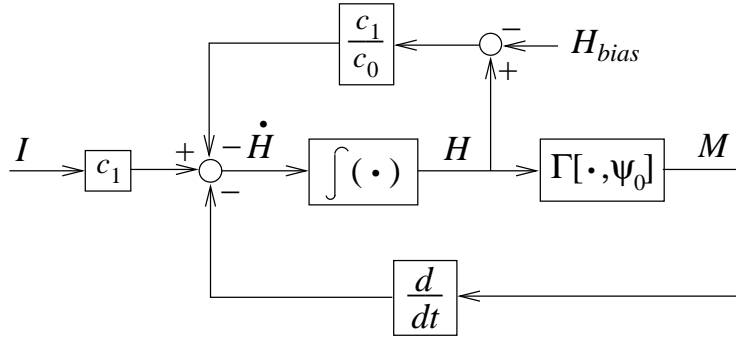
Figure 15: The block diagram of the block $\bar{W}$.

We note that the model (19) and (20) degenerates to the rate-independent model in Section 3 if we set the derivatives in these equations to 0.

In (19), the Preisach operator is coupled to an ordinary differential equation (ODE) in an unusual way. Eq. (19) can be viewed as a special nonlinear feedback system (Figure 15), and it presents interesting problems in analysis and computation [24].

The following theorem shows that the model (19) is well-posed. The proof can be found in [24, 22].

Theorem 4.1 *If the Preisach measure ν is nonnegative and nonsingular, and $I(\cdot)$ is piecewise continuous, then for any initial memory curve ψ_0, for any $T > 0$, there exists a unique pair $\{H(\cdot), M(\cdot)\} \in C([0,T]) \times C([0,T])$ satisfying (19) almost everywhere.*

4.2   Identification of the dynamic model

We can identify a discrete approximation to the Preisach measure using the scheme presented in Subsection 3.1. Furthermore, we can obtain a nonsingular Preisach measure from the collection of identified weighting masses by distributing each mass uniformly over the corresponding cell in the discretization grid, as discussed in Subsection 3.3. This is important since the well-posedness of (19) requires the Preisach measure to be nonsingular.

The following parameters, in addition to those listed in Subsection 3.1, are available from the manufacturer: $N_m = 1300$, $A_m = 2.83 \times 10^{-5} \mathrm{m}^2$. To estimate the first resonant frequency, we apply sinusoidal inputs of the same amplitude but different frequencies and measure the amplitudes
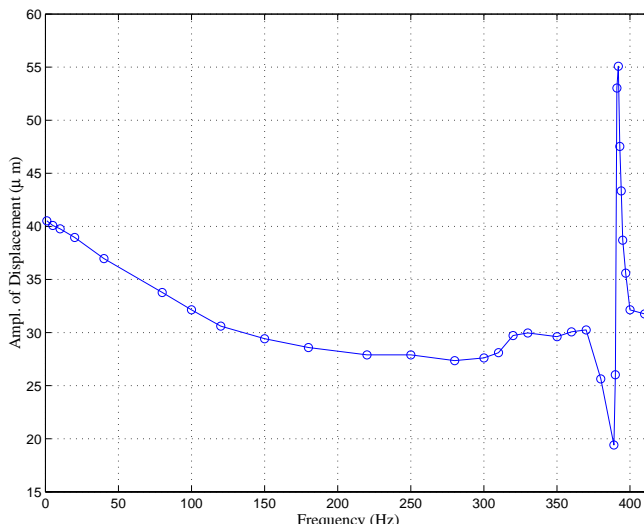
Figure 16: Displacement amplitude *vs.* input frequency.

of the displacement. Figure 16 displays the displacement amplitudes at different frequencies and we determine the first resonant frequency to be 392 Hz.

The most difficult parameters to identify are R_{eddy} and ξ due to the coupling of (19) and (20). A theoretical value of R_{eddy} can be computed with the formula $R_{eddy} = \frac{8\pi\rho N_m^2(b^2-a^2)}{l_m(b^2+a^2)}$ [4], where ρ is the resistivity of the magnetostrictive material, b and a are the outer and inner radii of the magnetostrictive rod. We obtain an upper bound $\bar{R}$ of R_{eddy} by letting $a = 0$. We then discretize $[0, \bar{R}]$ and denote the mesh points by $R_{eddy}^{(i)}$, $i = 1, \cdots, N$. The discretization need not be uniform and we make it finer in the region where the dynamics of (19) is more sensitive to R_{eddy}.

We observe a periodic motion of the actuator head when a periodic input is applied. The existence of periodic solutions of the model under periodic forcing has been proved in [24]. In addition, numerical simulation shows that the steady-state solution of (19) and (20) is periodic when $I(\cdot)$ is. These observations motivate the following scheme to identify R_{eddy} and ξ:

- **Step 1.** We apply a sinusoidal current (with some dc shift) $I(\cdot)$ with frequency f to the actuator and measure the phase lag $\theta_{y,I}$ between the fundamental frequency component of $y(\cdot)$ and $I(\cdot)$;

- **Step 2.** For each $R_{eddy}^{(i)}$, we numerically integrate (19) with $I(\cdot)$ as the input, and calculate the phase lag $\theta_{M^2,I}$ between the fundamental frequency component of $M^2(\cdot)$ and $I(\cdot)$.

- **Step 3.** The difference $\theta_{y,I} - \theta_{M^2,I}$ is considered to be the phase lag between the fundamental

22

frequency component of $y(\cdot)$ and that of $M^2(\cdot)$ in (20), from which we can compute $\xi^{(i)}$.

Remark 4.2 *The idea of relating the phase shift between the output and the input to hysteresis can also be found in [34]. We note that in general, the phase lag depends highly nonlinearly on the initial conditions (and the amplitude and frequency of $I(\cdot)$), so we should make sure that the initial conditions in numerical simulation are consistent with experiment conditions.*

We repeat the above procedure (Step 1 to Step 3) K times with different input frequencies and denote the damping coefficients as $\{\xi_k^{(i)}\}_{k=1}^K$ for $R_{eddy}^{(i)}$. If $R_{eddy}^{(i)}$ is close to the true parameter R_{eddy}, $\xi_k^{(i)}$ should not vary much with k. Therefore, we pick $i^* \in \{1, \cdots, N\}$ such that $\{\xi_k^{(i^*)}\}_{k=1}^K$ has the minimum variance, and estimate R_{eddy} via $R_{eddy} = R_{eddy}^{(i^*)}$ and let ξ be the mean of $\{\xi_k^{(i^*)}\}_{k=1}^K$.

Figure 17 shows the variation of ξ with respect to frequency for different $R_{eddy}^{(i)}$'s. The parameters are determined to be $R_{eddy} = 70\Omega$, $\xi = 0.7783$. Figure 18 compares the rate-dependent hysteresis loops measured in experiments to those obtained through simulation based on the identified parameters. We see that the simulation results agree with the experimental results reasonably well up to 200 Hz. Beyond 200 Hz, they still qualitatively agree although they match worse. This reveals that further details of the eddy currents and the magnetoelastic dynamics need to be brought into the picture to fully capture the dynamic behaviors at very high frequency.
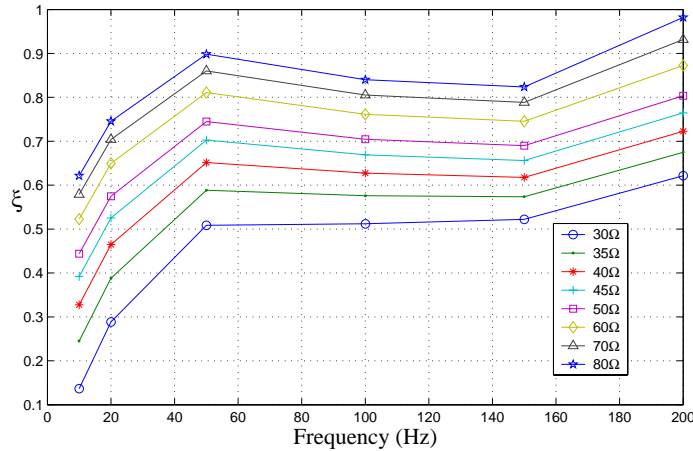

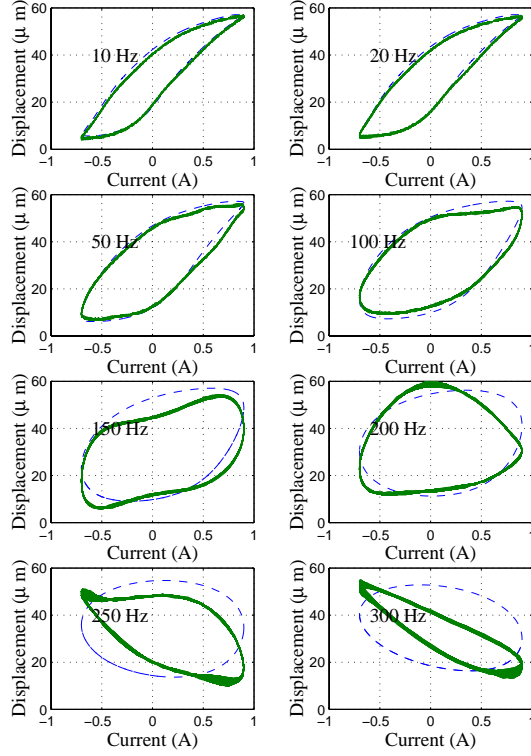Figure 17: Identification of R_{eddy} and ξ.

Figure 18: Model validation. Solid line: experimental measurement; Dashed line: numerical prediction based on the identified parameters.

4.3 Inversion of the dynamic model

Given an initial memory curve $\psi_0 \in \Psi$ and a desired trajectory $\bar{M}(\cdot)$ (obtained, e.g., as an output of $K(s)$ in Figure 9), the inversion problem for (19) is to find $I(\cdot)$, such that the corresponding output of $\bar{W}$ is $\bar{M}(\cdot)$.

We propose the following (formal) inverse scheme for (19):

$$\begin{cases} \bar{H}(t) = \Gamma^{-1}[\bar{M}(\cdot), \psi_0](t) \\ I(t) = \frac{1}{c_1}(\dot{\bar{H}}(t) + \dot{\bar{M}}(t)) + \frac{\bar{H}(t) - H_{bias}}{c_0} \end{cases} . \tag{21}$$

Due to the uniqueness of solution to (19), we expect the output $M(\cdot)$ under $I(\cdot)$ to agree with $\bar{M}(\cdot)$.

In implementation, we can use the schemes discussed in Section 3 for inversion of the Preisach operator (the first equation in (21)), and $\dot{\bar{M}}$ and $\dot{\bar{H}}$ in the second equation in (21) are approximated by the finite difference method.

Trajectory tracking experiments have been carried out to validate the model and examine the performance of the inverse scheme (21). To highlight the idea of inverse control, we have picked $\bar{y}(\cdot)$ from the space of attainable output trajectories $y(\cdot)$ of $G(s)$ (recall (20)) under some control $u(\cdot) \in C([0,T])$ with $0 \leq u(t) \leq M_s^2$, $\forall t \in [0,T]$. In this case, $\bar{M}$ can be directly computed as: $\forall t$, $\bar{M}(t) = \sqrt{\bar{u}(t)}$, where

$$\bar{u}(t) = \frac{M_s^2}{\omega_0^2 l_m \lambda_s}(\ddot{\bar{y}}(t) + 2\xi\omega_0\dot{\bar{y}}(t) + \omega_0^2\bar{y}(t)).$$

We compare the inverse control scheme (21) based on the dynamic model with a proportional feedback scheme and two other inverse schemes. For the other two inverse schemes, the first one is based on the static hysteresis model in Section 3, and the second one is based on a non-hysteretic model where the input-output relationship is approximated by a single-valued function

$$y(t) = -7.44I^3(t) - 2.63I^2(t) + 40.81I(t) + 30.34. \tag{22}$$

The non-hysteretic model (22) was obtained through the least squares method.

Experimental results are shown in Figures 19-22. The sampling period used was 5×10^{-5} second. In each figure, the displacement trajectories (both the desired and the measured), the tracking error, and the input current applied are displayed. We can see that the performance of the inverse control scheme based on the dynamic hysteresis model is very satisfactory (Figure 19). Although the controller parameter has been carefully tuned, the performance of the pure feedback scheme is poor (Figure 20). This highlights the need for hysteresis compensation. The other two inverse schemes also perform worse than the scheme (21), as one can see in Figure 21 and Figure 22.
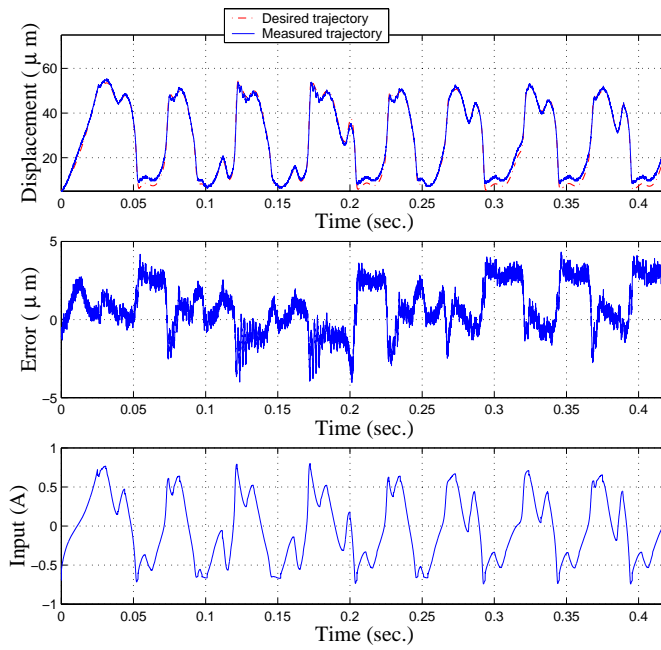
Figure 19: Experimental results of trajectory tracking using inverse control based on the dynamic hysteresis model.
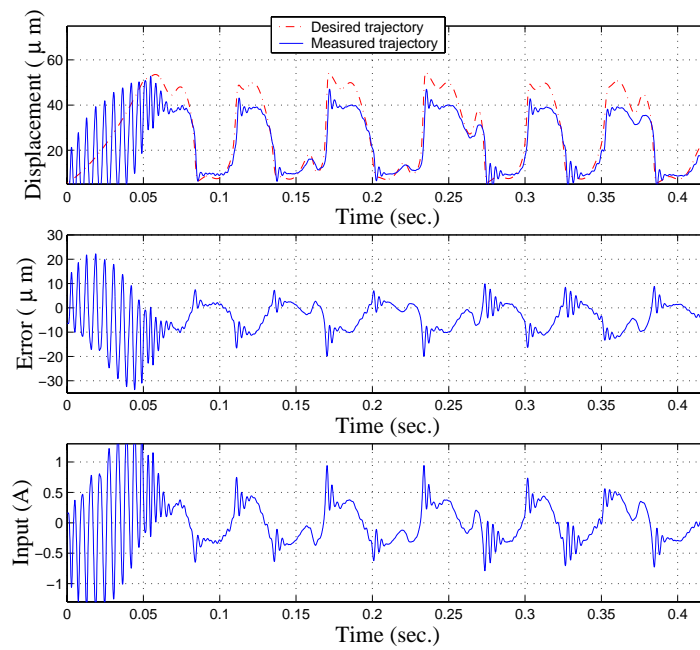

Figure 20: Experimental results of trajectory tracking using proportional feedback control.
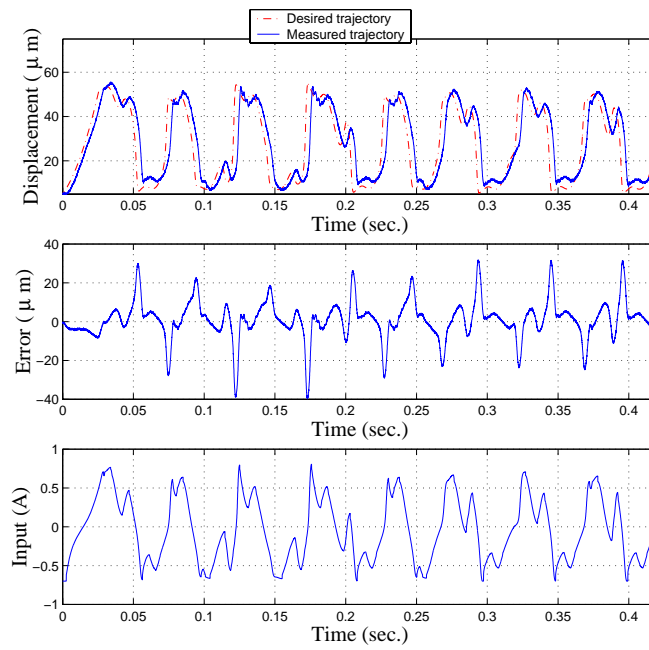
Figure 21: Experimental results of trajectory tracking using inverse control based on the static hysteresis model.
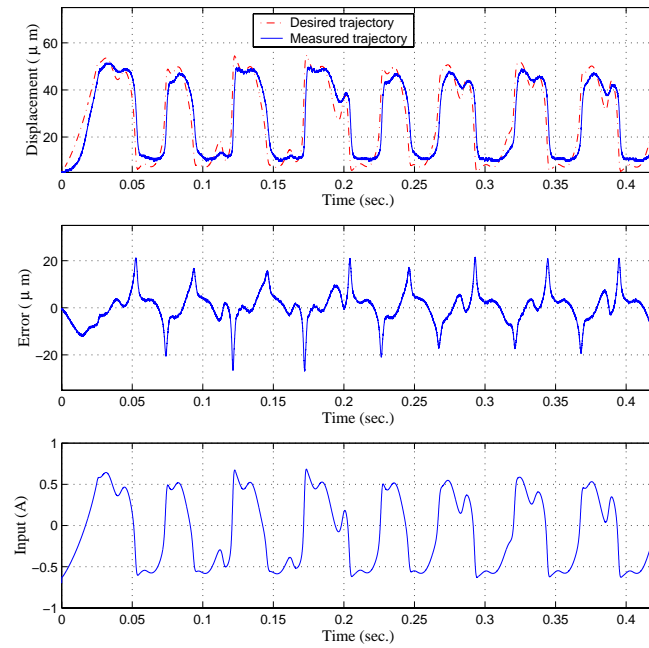

Figure 22: Experimental results of trajectory tracking using inverse control based on the non-hysteretic model.

5   Conclusions

In this paper we studied modeling, identification and control of hysteresis in smart actuators through the example of controlling a commercially available magnetostrictive actuator.

Hysteresis in a number of smart materials can be modeled by the Preisach operator. We developed fast inversion algorithms for the Preisach operator by exploiting structures and properties of the Preisach operator. We also presented a novel dynamic model for the rate-dependent magnetostrictive hysteresis. This model provides insight into modeling of rate-dependent hysteresis in other smart materials in the frequency ranges of practical interest. Parameter identification and inverse compensation for the dynamic model were also discussed in detail. Extensive experimental results have shown that the model we proposed can capture the hysteretic and dynamic behaviors of the actuator, and that our identification and inverse control schemes are effective. It is noteworthy that we achieved almost perfect tracking of an irregular and relatively high frequency signal for the full operating range of the actuator.

The approaches presented in this paper are very general and they are applicable to control of a wide class of smart actuators.

Due to the open loop nature of the inverse control scheme, its performance is susceptible to model uncertainties and to errors introduced by the inversion schemes. To address this problem, we have combined inverse compensation with the l_1 robust control theory and proposed a robust control framework for smart actuators. This will be reported in [2].

References

[1] S. O. R. Moheimani and G. C. Goodwin, "Guest editorial introduction to the special issue on dynamics and control of smart structures," *IEEE Transactions on Control Systems Technology*, vol. 9, no. 1, pp. 3–4, 2001.

[2] X. Tan and J. S. Baras, "Control of hysteresis in smart actuators, Part II: A robust control framework," submitted to *Automatica*, 2002.

[3] Etrema Products, Inc., Ames, IA, *Etrema Terfenol-D magnetostrictive actuators specifications and dimensions*, available at http://www.etrema-usa.com.

[4] R. Venkataraman, *Modeling and Adaptive Control of Magnetostrictive Actuators*, Ph.D. thesis, University of Maryland, College Park, 1999.

[5] D. Hughes and J. T. Wen, "Preisach modeling and compensation for smart material hysteresis," in *Active Materials and Smart Structures*, G. L. Anderson and D. C. Lagoudas, Eds., 1994, vol. 2427 of *SPIE*, pp. 50–64.

[6] G. Tao and P. V. Kokotović, "Adaptive control of plants with unknown hysteresis," *IEEE Transactions on Automatic Control*, vol. 40, no. 2, pp. 200–212, 1995.

[7] R. C. Smith, "Inverse compensation for hysteresis in magnetostrictive transducers," Tech. Rep. CRSC-TR98-36, CRSC, North Carolina State University, 1998.

[8] W. S. Galinaitis and R. C. Rogers, "Control of a hysteretic actuator using inverse hysteresis compensation," in *Mathematics and Control in Smart Structures*, V.V. Varadan, Ed., 1998, vol. 3323 of *SPIE*, pp. 267–277.

[9] X. Tan, R. Venkataraman, and P. S. Krishnaprasad, "Control of hysteresis: Theory and experimental results," in *Modeling, Signal Processing, and Control in Smart Structures*, V. S. Rao, Ed., 2001, vol. 4326 of *SPIE*, pp. 101–112.

[10] C. Natale, F. Velardi, and C. Visone, "Modelling and compensation of hysteresis for magnetostrictive actuators," in *Proceedings of IEEE/ASME International Conference on Advanced Intelligent Mechatronics*, 2001, pp. 744–749.

[11] M. A. Krasnosel'skii and A. V. Pokrovskii, *Systems with Hysteresis*, Springer-Verlag, 1989.

[12] I. D. Mayergoyz, *Mathematical Models of Hysteresis*, Springer Verlag, 1991.

[13] A. Visintin, *Differential Models of Hysteresis*, Springer, 1994.

[14] M. Brokate and J. Sprekels, *Hysteresis and Phase Transitions*, Springer Verlag, New York, 1996.

[15] E. Della Torre, *Magnetic Hysteresis*, IEEE Press, Piscataway, NJ, 1999.

[16] D. C. Jiles and D. L. Atherton, "Theory of ferromagnetic hysteresis," *Journal of Magnetism and Magnetic Materials*, vol. 61, pp. 48–60, 1986.

[17] A. A. Adly, I. D. Mayergoyz, and A. Bergqvist, "Preisach modeling of magnetostrictive hysteresis," *Journal of Applied Physics*, vol. 69, no. 8, pp. 5777–5779, 1991.

[18] D. Hughes and J. T. Wen, "Preisach modeling of piezoceramic hysteresis; independent stress effect," in *Mathematics and Control in Smart Structures*, V. V. Varadan, Ed., 1995, vol. 2442 of *SPIE*, pp. 328–336.

[19] P. Ge and M. Jouaneh, "Tracking control of a piezoceramic actuator," *IEEE Transactions on Control Systems Technology*, vol. 4, no. 3, pp. 209–216, 1996.

[20] R. B. Gorbet, D. W. L. Wang, and K. A. Morris, "Preisach model identification of a two-wire SMA actuator," in *Proceedings of IEEE International Conference on Robotics and Automation*, 1998, pp. 2161–2167.

[21] H. T. Banks, A. J. Kurdila, and G. Webb, "Identification of hysteretic control influence operators representing smart actuators, Part I: Formulation," *Mathematical Problems in Engineering*, vol. 3, no. 4, pp. 287–328, 1997.

[22] X. Tan and J. S. Baras, "Modeling and control of a magnetostrictive actuator," in *the Proceedings of the 41st IEEE Conference on Decision and Control*, Las Vegas, NV, 2002, pp. 866–872.

[23] H. L. Royden, *Real Analysis*, Prentice Hall, Englewood Cliffs, NJ, 1988.

[24] X. Tan, *Control of Smart Actuators*, Ph.D. thesis, University of Maryland, College Park, MD, Sept. 2002, available online at http://techreports.isr.umd.edu/TechReports/ISR/2002 /PhD_2002-8/PhD_2002-8.phtml.

[25] K.-H. Hoffmann, J. Sprekels, and A. Visintin, "Identification of hysteretic loops," *Journal of Computational Physics*, vol. 78, pp. 215–230, 1988.

[26] K.-H. Hoffmann and G. H. Meyer, "A least squares method for finding the Preisach hysteresis operator from measurements," *Numerische Mathematik*, vol. 55, pp. 695–710, 1989.

[27] M. J. Dapino, *Nonlinear and Hysteretic Magnetomechanical Model for Magnetostrictive Trans-ducers*, Ph.D. thesis, Iowa State University, Ames, Iowa, 1999.

[28] S. Chikazumi, *Physics of Magnetism*, John Wiley & Sons, Inc., 1966.

[29] W. F. Brown, *Magnetoelastic Interactions*, Springer-Verlag, 1966.

[30] R. Venkataraman and P. S. Krishnaprasad, "Approximate inversion of hysteresis: theory and numerical results," in *Proceedings of the 39th IEEE Conference on Decision and Control*, Sydney, Australia, Dec. 2000, pp. 4448–4454.

[31] W. S. Galinaitis and R. C. Rogers, "Compensation for hysteresis using bivariate Preisach models," in *Mathematics and Control in Smart Structures*, V. V. Varadan and J. Chandra, Eds., 1997, vol. 3039 of *SPIE*, pp. 538–547.

[32] D. P. Bertsekas, *Dynamic Programming and Optimal Control*, Athena Scientific, Belmont, Massachusetts, 1995.

[33] R. Venkataraman and P. S. Krishnaprasad, "A model for a thin magnetostrictive actuator," in *Proceedings of the 32nd Conference on Information Sciences and Systems, Princeton, NJ*, Princeton, Mar. 1998.

[34] J. M. Cruz-Hernández and V. Hayward, "Phase control approach to hysteresis reduction," *IEEE Transactions on Control Systems Technology*, vol. 9, no. 1, pp. 17–26, 2001.